Eur. Phys. J. A (2024) 60:95
https://doi.org/10.1140/epja/s10050-024-01318-2

THE EUROPEAN PHYSICAL JOURNAL A

Special Article - New Tools and Techniques

The first in-beam reaction measurement at CRYRING@ESR using the CARME array

Jordan J. Marsh[1,a], Carlo G. Bruno[1,b], Thomas Davinson[1], Philip J. Woods[1], Zoran Andelkovic[2], Angela Bräuning-Demian[2], Rui-Jui Chen[2,3], Sophia F. Dellmann[4], Phillip Erbacher[4], Svetlana Fedotova[2], Oliver Forstner[2,5], David Freire-Fernandez[6,7], Jan Glorius[2], Alexandre Gumberidze[2], Oscar Hall[1], Pierre-Michel Hillenbrand[8], Frank Herfurth[2], George Hudson-Chang[2,9], Anton Kalinin[2], Michael Lestinsky[2], Yuri A. Litvinov[2], Esther B. Menz[2], Chiara Nociforo[2], Nikolaos Petridis[2], Athanasios Psaltis[10], Shahab Sanjari[2,11], Mariia Selina[11], Uwe Spillman[2], Ragandeep S. Sidhu[1], Thomas Stöhlker[2,5], Laszlo Varga[1,2], Gleb Vorobjev[2]

[1] School of Physics and Astronomy, The University of Edinburgh, Peter Guthrie Tait Road, Edinburgh EH9 3FD, UK
[2] GSI Helmholtzzentrum für Schwerionenforschung, Planckstr. 1, 64291 Darmstadt, Germany
[3] CAS Key Laboratory of High Precision Nuclear Spectroscopy, Lanzhou, China
[4] Goethe University, Frankfurt, Germany
[5] Helmholtz-Institute Jena, Fröbelstieg 3, 07743 Jena, Germany
[6] Ruprecht-Karls-University, Heidelberg, Germany
[7] Max-Planck-Institut für Kernphysik, Heidelberg, Germany
[8] Physikalisches Institut, Justus-Liebig-Universität, 35392 Giessen, Germany
[9] RIKEN, Nishina Center for Accelerator-Based Science, Saitama, Japan
[10] TU Darmstadt, Darmstadt, Germany
[11] Aachen University of Applied Sciences, Aachen, Germany

Received: 12 February 2024 / Accepted: 12 April 2024

Communicated by Aurora Tumino

Abstract In the last decade nuclear reaction measurements using heavy ion storage rings became an important tool for nuclear astrophysics studies. The new CRYRING Array for Reaction MEasurements (CARME), recently commissioned at the low energy CRYRING@ESR storage ring (GSI/FAIR), is designed to take this novel approach one step further and perform direct nuclear reaction measurements at stellar energies, as well as indirect studies of nuclear properties of interest for nuclear astrophysics. CRYRING is unique worldwide in being able to store high quality, isotopically pure, radioactive beams produced in-flight at the low energies required for nuclear astrophysics. This paper describes the first in-beam reaction measurement with CARME at CRYRING, the first beam on (conventional) target measurement for FAIR Phase-0, and the data analysis approach required by this unprecedented, unique experimental approach.

1 Introduction

Nuclear reaction studies using heavy ion storage rings present a new and promising approach to probing nuclear reactions at the low energies relevant for nuclear astrophysics. Nuclear reaction measurements are now regularly performed utilising the Experimental Storage Ring (ESR) at the GSI/FAIR facility (Germany) [1–3] and have been conducted using the Cooler Storage Ring at the Heavy Ion Research Facility (HIRF-CSR) in Lanzhou (China) [4], however, measurements on these rings are limited to energies above a few MeV/u. The CRYRING, with its extreme high vacuum conditions (XHV, 10^{-11}–10^{12} mbar) and high magnetic stability at low energies, is capable of circulating ion beams at significantly lower energies (~ 100 keV/u), ideal for nuclear reaction measurements near and below the Coulomb barrier. The CRYRING Array for Reaction MEasurements (CARME) was recently installed on the CRYRING for this purpose [5]. CARME can house up to four high-resolution Double Sided Silicon strip Detectors (DSSDs) which feature 128 x by 128 y strips for a total of 16,384 pixels each, and are 100×100 mm^2 wide and 1 mm thick. The typical strip width is around 0.7 mm. These DSSDs are used to measure the products from the investigated reaction. Two sets of DSSDs

[a] e-mail: jordan.marsh@ed.ac.uk
[b] e-mail: carlo.bruno@ed.ac.uk (corresponding author)

Published online: 29 April 2024

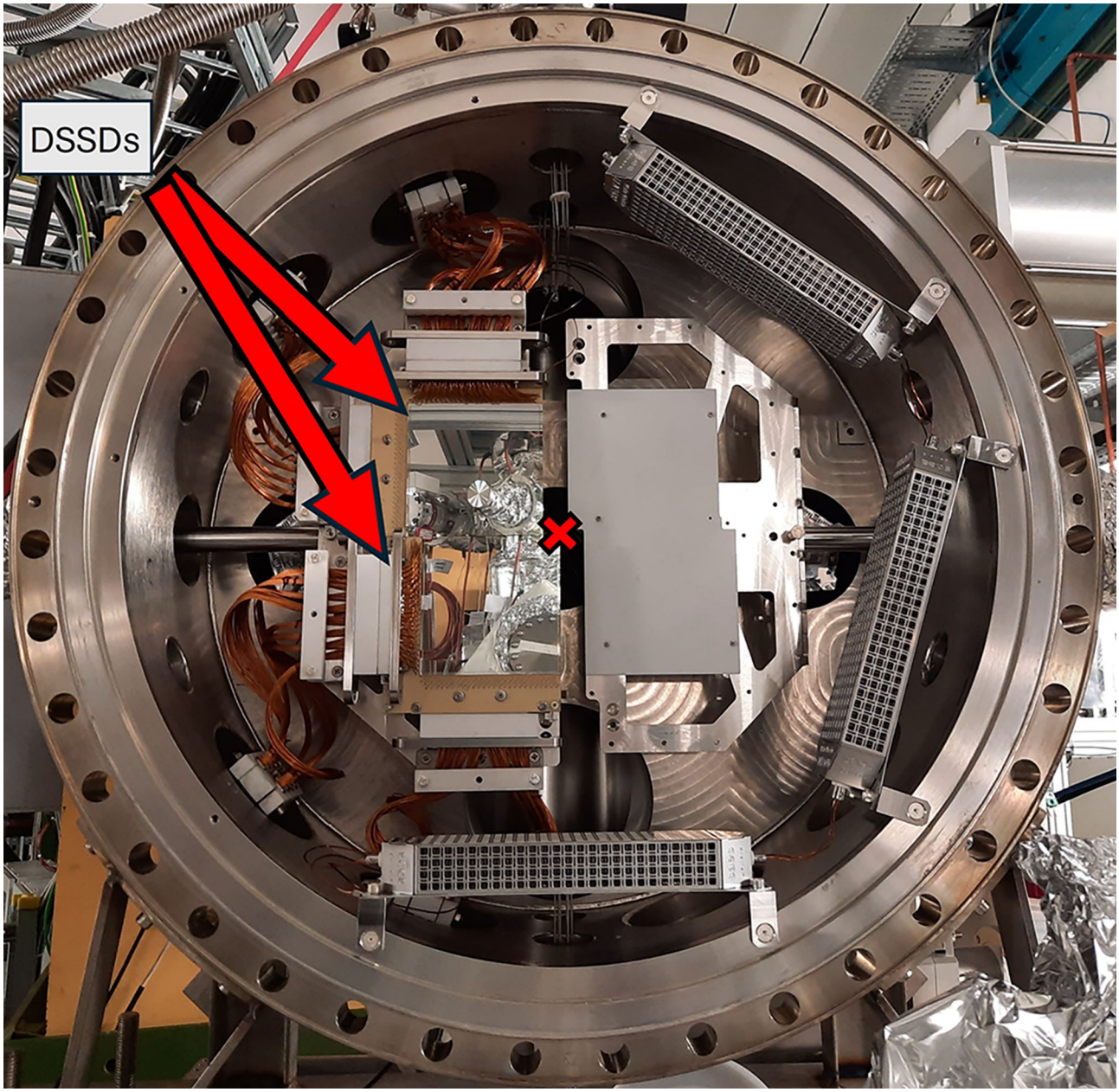

Fig. 1 A photo of the two moving DSSDs mounted on the left actuator arm in CARME. No DSSDs were mounted on the right actuator arm during the first measurement, but the support structure for these DSSDs is shown in the photo. The detectors are positioned fully in, as close as possible to the beam axis. The cooled beam, labelled with a cross in the image, goes into the page through the small gap in the centre of the array. Kapton wrapped cables carry signals from the detectors to XHV signal feedthroughs

can be mounted in CARME, forming an array of four detectors which are *moved periodically* during the experiment (see Fig. 1). The moving detectors are located close to the circulating beam covering angles $\lesssim 10$ degrees in the laboratory frame, and are ideal for high resolution angular distribution measurements performed in inverse kinematics. Details of the instrumentation included in CARME and the required procedures to achieve XHV with such instrumentation can be found in reference [5]. In this paper we describe the in-beam commissioning of CARME using a $^{2}H^{+}$ beam impinging on a ^{14}N internal target [6]. We commissioned CARME using elastic scattering data, and we detected reaction products from the $^{14}N(d,p)^{15}N$ and $^{14}N(d,\alpha)^{12}C$ reactions, the first nuclear reactions to be ever studied at CRYRING.

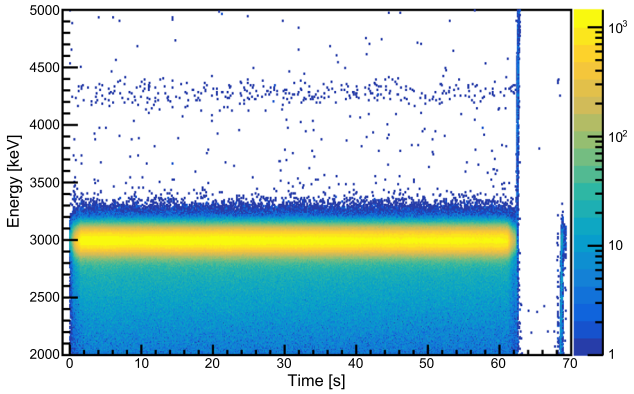

Fig. 2 Detected energy against time plot showing the events observed by CARME over the measurement cycle time. The plot is a sum of 1040 ring cycles. Time t=0 corresponds to the detector beginning to move in. The measurement time is between 2 and 60 s. The beam is dumped at ∼ 60 s before re-injection ∼5 s later

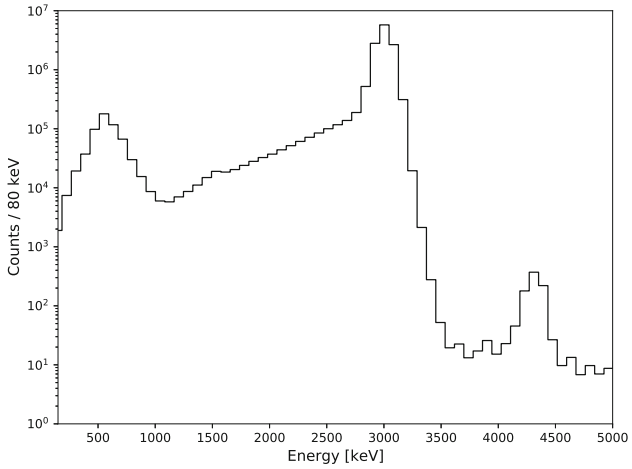

Fig. 3 Energy spectrum below 5 MeV acquired at a beam energy of 1.5 MeV/u integrated across all angles. Only accepted events when the detectors were stationary and cooled beam is interacting with the target are considered. See text for further details. Elastic scattering (3 MeV) is the dominant process observed. Above the elastic peak events from the ^{14}N(d, p)^{15}N reaction can be seen. Other nuclear products from the ^{14}N+d reaction can be seen in Fig. 5

2 Methodology

2.1 Measurement cycle

This first reaction study was carried out with a $^{2}H^{+}$ beam extracted from the local CRYRING MINIS ion source, and injected at 300 keV/u into the CRYRING via a radio-frequency quadrupole. About 10^{7} ions were injected and then accelerated to an energy of 1.5 MeV/u, at which they circulated around the ring with a revolution frequency of about 3×10^{5} Hz. Once per revolution, the beam interacted with a nitrogen gas-jet target with a density of about 10^{11} atoms/cm^{2}. When the beam is first injected into the ring, due to its relatively large emittance and width, the moving detectors must be moved away from the beam axis. After the beam has been accelerated to the energy of interest, and then cooled via the CRYRING ultra-cold electron cooler [7], the beam width is reduced to several millimetres and the detectors are moved towards the beam axis. The beam is stored and the reaction of interest is measured until interactions with the target and residual gases reduce the beam intensity to the point where it is more efficient to dump the beam and re-inject at the original beam intensity. Before the beam is dumped from the ring, the detectors are moved away from the beam axis.

For this first experiment, the total time between consecutive beam injections was about 70 s, of which around 58 seconds were used to measure the reaction and 12 s were used to prepare the beam. The energy of events against the time in the ring cycle the event was detected, for a total 1040 cycles (∼ 20 h of beamtime), is shown in Fig. 2. Time zero is set to the moment when the detector is given the instruction to move in, after the beam has been cooled. During the first two seconds the detector is moving towards the beam axis. Between approximately 2 and 60 s the detector remains stationary while the beam circulates around the ring and interacts with the target. Finally, the detector is moved away before the beam is dumped from the ring at approximately 60 s. Re-injection occurs ∼ 5 s later. In this measurement we expected the beam intensity to be reduced by $< 5\%$ during the measurement period due to the relatively high beam energies and low Z of the deuterium beam. The majority of events detected throughout the cycle are from elastic scattering (3 MeV). A spike in events with a range of energies that extend above that of elastic scattering was observed when the beam is dumped from the ring at ∼ 60 s, in addition to some low energy events (< 1 MeV) during the movement of the detectors. Events associated with the dumping of beam from the ring were also observed in experimental runs where the detector was kept stationary throughout, and are likely due to scattering of un-cooled beam, electronic pickup from the ring RF elements or rapid changes in magnetic/electric fields in the ring during the dumping of the beam. Removing these non-physical events requires accurately separating the different phases in the ring cycle in order to consider only the time period when the detector is stationary and cooled beam is incident on the target. Different ring phases are identified using signals independently sent to the data acquisition system whenever the detector starts or stops moving, i.e. four times for each measurement cycle.

An energy spectrum for this selected measurement period (2–60 s) for events below 5 MeV, integrated across all detection angles, is shown in Fig. 3. Note the dominant elastic scattering peak at 3 MeV, its tail, and a clearly visible peak from one excited state of the ^{14}N(d,p)^{15}N reaction. In addition to event rejection based on the time in the ring cycle, individual

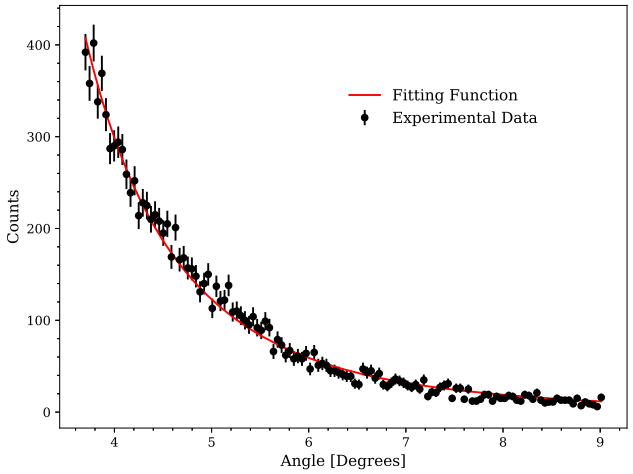

Fig. 4 Plot of the number of counts in the elastic peak ($2800 \leq E \leq 3200$ keV) across a single y strip. In red is the fitting function when χ^2 is minimised

strips were examined to ensure no electronic anomalies are present.

2.2 Energy and position calibrations

CARME utilises AIDA [8] for the electronics readout and data acquisition. The energy calibration was performed in two steps. First, the offset was determined via a pulser walk-through. Then, the gain was obtained using the elastic scattering peak which has a known energy around 3 MeV depending on the detection angle. Elastic scattering was also used to determine the position of the moving detectors relative to the circulating beam. The relative displacement of the DSSD across the beam axis is monitored by a string potentiometer which has a precision of 0.1 mm [5]. However, the absolute position of the DSSD from the beam must be determined during each experimental beamtime. The high segmentation of the DSSD and the well known angular dependency of Rutherford scattering, which dominates the rate at the energy and angular range covered by CARME, provide a robust method to determine the position of the detector from the beam. The DSSD is highly segmented with 128 horizontal (x) and 128 vertical (y) strips. The position of the detectors across the beam axis (x coordinate) is found by considering the elastic scattering rate across five y strips separately. These strips are close to the nominal height of the beam. The energy of the events considered is limited to only those inside the elastic scattering peak ($2800 \leq \mathrm{E} \leq 3200$ keV for this measurement). The elastic count rate across all pixels across a given y strip is plotted as a function of the angle, and fitted with the Rutherford angular distribution function. At the distance of the DSSD from the interaction point (~ 1 m), each pixel covers a laboratory angle of about 0.05°. Fitting is performed for the range of possible detector positions. The detector position is determined by minimising the χ^2. The uncertainty in the detector position is estimated by the position change at $\chi^2{}_{min} + 1$ from the fitting function. The final position is calculated using the average of the five strips considered. Figure 4 shows the number of elastic scattering counts across a single strip and the fitting function where χ^2 is minimised. Total uncertainties on the x position of the detector of ~ 0.1 mm were achieved for experimental runs with a large number of detected elastic scattering counts during the commissioning beam time. The detector positions determined using this method were consistent with the potentiometer displacement between different experimental runs using the same beam settings. The position of the detectors in the y axis is determined by finding the y strip with the highest number of elastic counts across the detector, as this strip will be at the same height as the circulating beam. This position was found to be consistent with mechanical drawings.

2.3 Cross-section normalisation

The detector position is mandatory for an accurate normalisation of cross sections using elastic scattering. The differential cross section for nuclear reaction measurements using CARME is given by

$$\frac{d\sigma}{d\Omega} = \frac{\mathrm{N}}{\mathrm{N}_b \mathrm{N}_t \eta f d\Omega} = \Lambda \frac{\mathrm{N}}{d\Omega} \tag{1}$$

where N is the number of detected particles across a solid angle of $\mathrm{d}\Omega$, N_b is the beam intensity, N_t is the number of target nuclei per unit area, η is the intrinsic detection efficiency, f is the revolution frequency. Note that in storage ring experiments the beam intensity changes over time as a result of beam loss and beam re-injection and the internal target density is not always stable. It is therefore convenient to introduce a normalisation parameter, Λ, that is a combination of the beam intensity, target density, revolution frequency and detection efficiency and that accounts for the varying luminosity of the experiment over time. This normalisation parameter is obtained from the magnitude of the elastic scattering by substituting for the Rutherford differential cross section in Eq. 1. The Rutherford scattering cross section is known with essentially no uncertainty. The main uncertainty on the normalisation comes from the geometric efficiency, i.e. the determination of the position of the moving detectors relative to the circulating beam. Due to the high angular dependence of the Rutherford cross section, the detector position is required with a precision ≤ 1 mm. The systematic uncertainty from the normalisation was $\leq 2\%$ for all experimental runs presented here, and statistical uncertainties of the detected nuclear reaction products presented in the next section dominate the results.

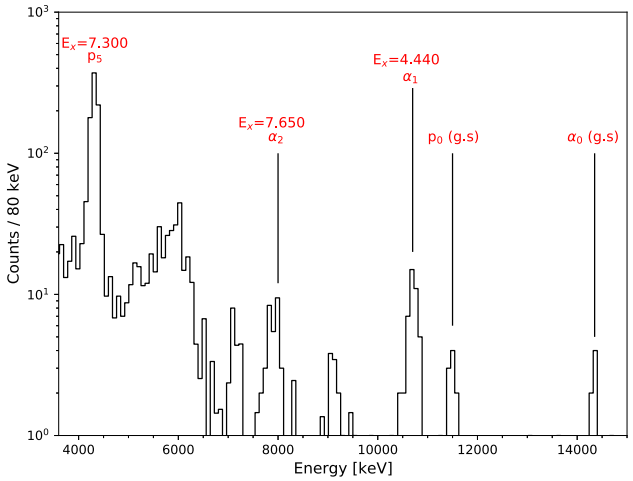

Fig. 5 Energy spectrum above the elastic scattering energies, integrated across all angles and all experimental runs at a beam energy of 1.5 MeV/u, for the period when detectors are stationary and beam is on target. Several states from the positive Q-value ^{14}N(d,p)^{15}N and ^{14}N(d,α)^{12}C reactions are labelled. Excitation energies are taken from the NuDAT database [9]. The broad structure between 5 and 7 MeV is attributed to several unresolved (d,p) and (d,α) excited states in addition to pile-up of scattering events

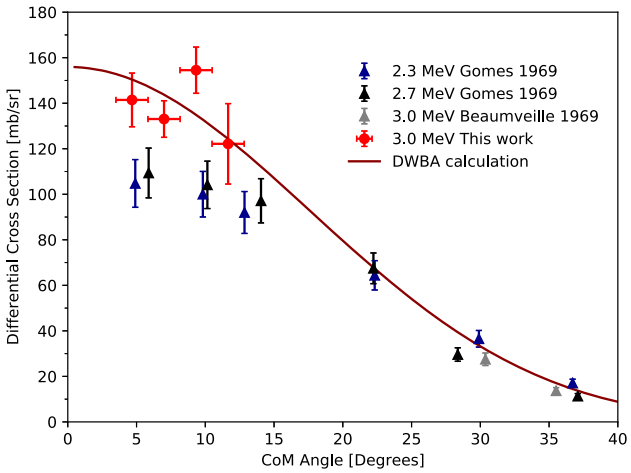

Fig. 6 Plot of the cross section for the ^{14}N(d, p$_5$)^{15}N reaction determined in this work compared to previous measurements by Gomes [10] at beam energies of 2.3 and 2.7 MeV and by Beaumeveille [11] at a beam energy of 3 MeV. The angular distribution calculated using the nuclear reaction code Fresco [15] is shown in red

3 Results

Protons and alpha particles from several different states populated by the ^{14}N(d,p)^{15}N and ^{14}N(d,α)^{12}C nuclear reactions were observed above the elastic scattering peak. Above the elastic scattering peak, the measurement is essentially background-free due to the pure ion beam and target. The peaks observed are identified and labelled with their excitation energies taken from the NuDAT database [9] in Fig. 5. The cross section of all identified (d,p) and (d,α) states are consistent with previous measurements in the same energy and angular range [10–13]. However, due to the low statistics of our measurement only the results for the ^{14}N(d, p)^{15}N reaction to the fifth excited state (E_x= 7.30 MeV) are included in this paper.

The unlabelled broad structure between 5 and 7 MeV is attributed to several unresolved (d,p) and (d,α) excited states in addition to pile-up of scattering events, which are focused at low angles on the edge of the detector. These states were unable to be resolved due to an energy resolution of 150 keV, far worse than expected due to electronic noise. Pile up of scattering events were identified from nuclear reaction products by the energy of events and also by separating events into specific angular bins i.e. 2–4 deg, 4–6 deg etc. Sources of background from radioactive decay chains and cosmic particles are characterised during background runs with no beam in the ring, and are subtracted from the final energy spectra. The highest number of counts observed was for the ^{14}N(d, p)^{15}N reaction to the fifth excited state. This state was populated even with very low beam energies by Valek et al. [14] who remarked that this transition is likely to be "almost entirely" direct. The high number of counts of this reaction, compared to the other reactions observed, results in the bench-marking of the CARME system being focused on this particular reaction. The differential cross section for this reaction at several angles compared to previous measurements by Gomes [10] and Beaumeveille [11] at similar beam energies to our measurement are shown in Fig. 6. The uncertainty in our measurements is dominated by the statistical uncertainty for each data point. The red line corresponds to DWBA calculations of the differential cross section using the nuclear reaction code Fresco [15]. Note that DWBA is very appropriate here since we are dealing with a primarily direct transition. The optical potentials used in the calculation are detailed in Table 1. The spectroscopic factor C^2S was extracted by comparison between the DWBA calculation and the experimental cross section using the relation

$$\left(\frac{d\sigma}{d\Omega}\right)_{exp} = C^2S\left(\frac{d\sigma}{d\Omega}\right)_{DWBA}. \quad (2)$$

The spectroscopic factor extracted from the comparison between our experimental measurements and the Fresco DWBA calculation, in addition to the spectroscopic factor determined in previous measurements is shown in Table 2. The uncertainty in the spectroscopic factor resulting from the χ^2 fitting (χ^2 + 1) to the experimental data is $\sim$ 5%, and we estimate an uncertainty of 5–10% arising from the choice of optical potential parameters in the DWBA calculation. Potential parameters were obtained from the OMP reference input parameter library [16] and are similar to those employed by Gomes [10], Beaumeveille [11] and Valek [14]. The spectroscopic factor extracted is in good agreement with

Table 1 Optical model potential (OMP) parameters used in Fresco DWBA calculation of the ^{14}N(d, p)^{15}N reaction. The potentials refer to the entrance and exit scattering channels, the transferred neutron and core–core interactions. Potential parameters were obtained from the OMP reference input parameter library [16]

Potential	V_v	r_v	a_v	W_v	r_{wv}	a_{wv}	W_D	r_D	a_D	V_{so}	r_{so}	a_{so}	r_c
^{14}N + d	94.0	1.15	0.65	1.30	1.35	0.61	10.7	1.40	0.68	3.60	0.97	1.01	1.30
^{15}N + p	61.0	1.06	0.65	1.60	1.37	0.77	5.00	1.37	0.77	6.00	1.06	0.78	1.25
^{14}N + n	47.4	1.25	0.68	0.00	1.39	0.45	4.40	1.26	0.51	7.00	1.31	0.66	1.30
^{14}N + p	51.9	1.16	0.75	1.30	1.37	0.77	5.00	1.37	0.77	6.00	1.06	0.78	1.25

Table 2 Table of spectroscopic factors determined in this work compared to previous studies. Spectroscopic factors reported by Gomes [10], Beaumeveille [11], Valek [14] and Phillips [17] are from experimental studies. The spectroscopic factor reported by MacFarlane [18] is from a theoretical calculation. Superscripts a and b denote the two different potentials (D3+P2) and (D4+P1) used in the DWBA calculations by Gomes

Reference	Spectroscopic factor
This measurement	0.66
Gomes[a] [10]	0.72
Gomes[b] [10]	0.70
Beaumeveille [11]	0.89
Valek [14]	0.72
Phillips [17]	0.89
MacFarlane [18]	0.64

previous studies, confirming the successful commissioning of CARME and of the data analysis procedure.

4 Future steps

This was the first in-beam measurement for CARME, as well as the first ever nuclear reaction studied at the CRYRING. Results from the commissioning with elastic scattering and transfer reactions are already excellent, and much can be improved still for future experiments.

In particular, it was the first time the CRYRING's internal target was ever turned on since the installation of CRYRING at GSI, and we were limited in the maximum target density achievable to around 10^{11} atoms/cm^2 due to technical difficulties, which was an order of magnitude lower than expected. It is expected densities up to 10^{14} atoms/cm^2 will be achievable in future measurements, just as they are at the ESR [19]. Furthermore, in this measurement, the target remained on throughout the experiment, including during injection and cooling phases. In future measurements, the target will only be turned on after the beam has been cooled to reduce beam loss due to beam-target interactions, and improve the ring vacuum increasing the beam lifetime and the luminosity.

Energy resolution and electronic noise can also be improved upon. While for this experiment we were able to clearly separate all reaction peaks, CARME had a resolution of around 150 keV FWHM, far worse than the 30 keV FWHM which should be achievable. This poor resolution was in large part due to our incomplete knowledge of this new system, and minor improvements in the grounding scheme of the electronics after this in-beam run improved the resolution to 70 keV FWHM already. Further improvements have been planned. Not only will this increase the resolution, but it will also allow us to improve noise rejection. In this experiment, we identified as noise and discarded events showing an energy difference greater than 200 keV (i.e. far larger than the FWHM) between the front and the back strips of the DSSD. In future experiments we will be able to tighten this energy difference cut.

Finally, the relatively limited statistics we acquired were due to the fact that only one DSSD out of a maximum of four was in use, and that only $\sim$ 51 h of beam could be delivered on the target, due to a mix of issues with the target itself and with the ion source. Future experiments will be making use of the full array of four DSSDs, a now-commissioned internal target, and a refurbished local ion source, and will achieve much better duty cycles and luminosities.

5 Conclusions

The first ever in-beam measurement was carried out using CARME at CRYRING. The novel analysis approach for CARME at CRYRING was defined and successfully tested using elastic scattering of ^{2}H$^+$ on a natural nitrogen target. In particular, the characteristics of the ring cycle are now well understood and the system has been calibrated in energy and position. The cross sections of the ^{14}N(d,p)^{15}N and ^{14}N(d,α)^{12}C nuclear reactions were successfully normalised to elastic scattering, and were found to be in agreement with previous measurements. This successful commissioning measurement provides a strong basis for the future physics programme using CARME.

Acknowledgements The results presented here are based on the experiment E141, which was performed at the infrastructure CRYRING at the GSI Helmholtzzentrum für Schwerionenforschung, Darmstadt, in the framework of FAIR Phase-0 and the SPARC collaboration. JJM and CGB are supported by the ELDAR (burning questions on the origin of the Elements in the Lives and Deaths of stARs) UKRI ERC StG (EP/X019381/1). JG, YAL and TS gratefully acknowledges support by the State of Hesse within the Research Cluster ELEMENTS (Project ID 500/10.006). PMH acknowledges the support provided by ErUM FSP T05-'Aufbau von APPA bei FAIR' (BMBF no. 05P21RGFA1). AP acknowledges support from Deutsche Forschungsgemeinschaft (DFG, German Research Foundation)-Project No. 279384907-SFB 1245.

Data Availability Statement Data will be made available on reasonable request.

Code availability Code/software will be made available on reasonable request.

References

1. B. Mei, T. Aumann, S. Bishop, K. Blaum, K. Boretzky, F. Bosch, C. Brandau, H. Bräuning, T. Davinson, I. Dillmann, C. Dimopoulou, O. Ershova, Z. Fülöp, H. Geissel, J. Glorius, G. Gyürky, M. Heil, F. Käppeler, A. Kelic-Heil, C. Kozhuharov, C. Langer, T. Le Bleis, Y. Litvinov, G. Lotay, J. Marganiec, G. Münzenberg, F. Nolden, N. Petridis, R. Plag, U. Popp, G. Rastrepina, R. Reifarth, B. Riese, C. Rigollet, C. Scheidenberger, H. Simon, K. Sonnabend, M. Steck, T. Stöhlker, T. Szücs, K. Sümmerer, G. Weber, H. Weick, D. Winters, N. Winters, P. Woods, Q. Zhong, First measurement of the ^{96}Ru$(p,\gamma)^{97}$Rh cross section for the p process with a storage ring. Phys. Rev. C **92**, 035803 (2015). https://doi.org/10.1103/PhysRevC.92.035803
2. J. Glorius, C. Langer, Z. Slavkovská, L. Bott, C. Brandau, B. Brückner, K. Blaum, X. Chen, S. Dababneh, T. Davinson, P. Erbacher, S. Fiebiger, T. Gaßner, K. Göbel, M. Groothuis, A. Gumberidze, G. Gyürky, M. Heil, R. Hess, R. Hensch, P. Hillmann, P.-M. Hillenbrand, O. Hinrichs, B. Jurado, T. Kausch, A. Khodaparast, T. Kisselbach, N. Klapper, C. Kozhuharov, D. Kurtulgil, G. Lane, C. Lederer-Woods, M. Lestinsky, S. Litvinov, Y.A. Litvinov, B. Löher, F. Nolden, N. Petridis, U. Popp, T. Rauscher, M. Reed, R. Reifarth, M.S. Sanjari, D. Savran, H. Simon, U. Spillmann, M. Steck, T. Stöhlker, J. Stumm, A. Surzhykov, T. Szücs, T.T. Nguyen, A. Taremi Zadeh, B. Thomas, S.Y. Torilov, H. Törnqvist, M. Träger, C. Trageser, S. Trotsenko, L. Varga, M. Volknandt, H. Weick, M. Weigand, C. Wolf, P.J. Woods, Y.M. Xing, Approaching the Gamow window with stored ions: direct measurement of ^{124}Xe(p,γ) in the ESR storage ring. Phys. Rev. Lett. **122**, 092701 (2019). https://doi.org/10.1103/PhysRevLett.122.092701
3. J. Glorius, C.G. Bruno, Low-energy nuclear reactions with stored ions: a new era of astrophysical experiments at heavy ion storage rings. Eur. Phys. J. A **59**(4), 81 (2023)
4. K. Yue, J.T. Zhang, X.L. Tu, C.J. Shao, H.X. Li, P. Ma, B. Mei, X.C. Chen, Y.Y. Yang, X.Q. Liu, Y.M. Xing, K.H. Fang, X.H. Li, Z.Y. Sun, M. Wang, P. Egelhof, Y.A. Litvinov, K. Blaum, Y.H. Zhang, X.H. Zhou, Measurement of ^{58}Ni$(p,p)^{58}$Ni elastic scattering at low momentum transfer by using the HIRFL-CSR heavy-ion storage ring. Phys. Rev. C **100**, 054609 (2019). https://doi.org/10.1103/PhysRevC.100.054609
5. C.G. Bruno, J.J. Marsh, T. Davinson, P.J. Woods, P. Black, A. Bräuning-Demian, J. Glorius, A. Grant, O. Hall, A. Headspith, P. Hindley, I. Lazarus, K. Middleman, N. Petridis, M. Lestinsky, Y.A. Litvinov, R.S. Sidhu, T. Stöhlker, CARME—the CRYRING Array for Reaction MEasurements: a new approach to study nuclear reactions using storage rings. Nucl. Instrum. Methods Phys. Res. Sect. A: Accel. Spectrom. Detect. Assoc. Equip. **1048**, 168007 (2023). https://doi.org/10.1016/j.nima.2022.168007
6. N. Petridis, M. Lestinsky, A. Kallberg, H.T. Schmidt, Y.A. Litvinov, R.E. Grisenti, Technical design report: the CRYRING internal jet target (2018). https://edms.cern.ch/ui/file/2059586/1/The_CRYRING_Internal_Jet_Target__submitted_2018-02-23__-_public_2018-11-01.pdf
7. M. Lestinsky, V. Andrianov, B. Aurand, V. Bagnoud, D. Bernhardt, H. Beyer, S. Bishop, K. Blaum, A. Bleile, A. Borovik, F. Bosch, C.J. Bostock, C. Brandau, A. Bräuning-Demian, I. Bray, T. Davinson, B. Ebinger, A. Echler, P. Egelhof, A. Ehresmann, M. Engström, C. Enss, N. Ferreira, D. Fischer, A. Fleischmann, E. Förster, S. Fritzsche, R. Geithner, S. Geyer, J. Glorius, K. Göbel, O. Gorda, J. Goullon, P. Grabitz, R. Grisenti, A. Gumberidze, S. Hagmann, M. Heil, A. Heinz, F. Herfurth, R. Heß, P.-M. Hillenbrand, R. Hubele, P. Indelicato, A. Källberg, O. Kester, O. Kiselev, A. Knie, C. Kozhuharov, S. Kraft-Bermuth, T. Kühl, G. Lane, Y.A. Litvinov, D. Liesen, X.W. Ma, R. Märtin, R. Moshammer, A. Müller, S. Namba, P. Neumeyer, T. Nilsson, W. Nörtershäuser, G. Paulus, N. Petridis, M. Reed, R. Reifarth, P. Reiß, J. Rothhardt, R. Sanchez, M.S. Sanjari, S. Schippers, H.T. Schmidt, D. Schneider, P. Scholz, R. Schuch, M. Schulz, V. Shabaev, A. Simonsson, J. Sjöholm, Ö. Skeppstedt, K. Sonnabend, U. Spillmann, K. Stiebing, M. Steck, T. Stöhlker, A. Surzhykov, S. Torilov, E. Träbert, M. Trassinelli, S. Trotsenko, X.L. Tu, I. Uschmann, P.M. Walker, G. Weber, D.F.A. Winters, P.J. Woods, H.Y. Zhao, Y.H. Zhang, Physics book: CRYRING@ESR. Eur. Phys. J. Spec. Top. **225**(5) (2016). https://doi.org/10.1140/epjst/e2016-02643-6
8. O. Hall, T. Davinson, C.J. Griffin, P.J. Woods, C. Appleton, C.G. Bruno, A. Estrade, D. Kahl, L. Sexton, I. Burrows, P.J. Coleman-Smith, M. Cordwell, A. Grant, M. Kogimtzis, M. Labiche, J. Lawson, I. Lazarus, P. Morall, V.F.E. Pucknell, J. Simpson, C. Unsworth, D. Braga, M. Prydderch, S.L. Thomas, L.J. Harkness-Brennan, P.J. Nolan, R.D. Page, D. Seddon, The advanced implantation detector array (AIDA). Nucl. Instrum. Methods Phys. Res. Sect. A: Accel. Spectrom. Detect. Assoc. Equip. (2023). https://doi.org/10.1016/j.nima.2023.168166
9. NNDC: NuDAT (2023). https://www.nndc.bnl.gov/nudat3/. Accessed 10/2023
10. V. Gomes Porto, N. Ueta, R.A. Dougles, O. Sala, D. Wilmore, B.A. Robson, P.E. Hodgson, Deuteron induced reactions on ^{14}N. Nucl. Phys. A **136**(2), 385–413 (1969). https://doi.org/10.1016/0375-9474(69)90060-8
11. H. Beaumevieille, M. Lambert, M. Yaker, A. Amokrane, N. van Sen, Study of the ^{14}N(d, d)^{14}N and ^{14}N(d, p)^{15}N angular distributions and excited states of ^{15}N. Nucl. Phys. **125**, 568–584 (1969)
12. N.A. Mansour, H.R. Saad, Z.A. Saleh, E.M. Sayed, I.I. Zaloubovsky, V.J. Gontchar, Studies of the (d, a) reaction on N14 in the deuteron energy range from 1 to 2.5 MeV. Nucl. Phys. **59**(2), 241–252 (1964). https://doi.org/10.1016/0029-5582(64)90081-1

13. A. Gallmann, P. Fintz, P.E. Hodgson, Réactions (d, p) sur ^{11}B, ^{12}C, ^{14}N et ^{16}O à Ed $\leq$ 5.5 MeV. Nucl. Phys. **82**(1), 161–181 (1966). https://doi.org/10.1016/0029-5582(66)90529-3
14. A. Valek, T. Vertse, B. Schlenk, I. Hunyadi, A study of the ^{14}N(d, p)^{15}N reaction at low bombarding energies. Nucl. Phys. A **270**(1), 200–210 (1976). https://doi.org/10.1016/0375-9474(76)90135-4
15. I. Thompson, Fresco (2023). http://www.fresco.org.uk/. Accessed 05/2023
16. Input Parameter Library, R (2023). https://www-nds.iaea.org/RIPL-3/. Accessed 05/2023
17. G.W. Phillips, W.W. Jacobs, Structure of ^{15}N and the ^{14}N$(d, p)^{15}$N reaction. Phys. Rev. **184**, 1052–1060 (1969). https://doi.org/10.1103/PhysRev.184.1052
18. M.H. Macfarlane, J.B. French, Stripping reactions and the structure of light and intermediate nuclei. Rev. Mod. Phys. **32**, 567–691 (1960). https://doi.org/10.1103/RevModPhys.32.567
19. M. Steck, Y.A. Litvinov, Heavy-ion storage rings and their use in precision experiments with highly charged ions. Prog. Part. Nucl. Phys. **115**, 103811 (2020). https://doi.org/10.1016/j.ppnp.2020.103811